Check for updates

Hydrophobic deep eutectic solvent-based eutectogels for long-term humidity resistance and multifunctional sensing

Qianwen Lu,[b] Hengfeng Li, [ID] *[b] Changyong Cai*[c] and Zhijian Tan [ID] *[a]

Eutectogels based on deep eutectic solvents (DESs) hold significant potential for application in flexible sensors. However, their hygroscopic nature limits their use in humid environments. In this study, a eutectogel with excellent long-term humidity resistance was developed *via* radical copolymerization of acrylic acid monomers in a hydrophobic DES (HES). The hydrophobicity of the HES makes the gel highly stable under humid conditions, with a water absorption rate of only 2.8% at 30 °C and 90% relative humidity over 30 d. Even after storage in a humid environment for 365 d, the gel maintained its tensile mechanical properties (retaining 99.3% of toughness) and shape. In addition, the gel exhibits several outstanding properties. Sensors fabricated from these gels demonstrate high sensitivity to strain, pressure, and temperature, along with excellent durability in humid environments. These sensors are capable of real-time monitoring of various human activities and deliver stable signal output. This work paves the way for the development of long-lasting gels and lays a foundation for the advancement and application of functional gel materials.

New concepts

Recently, the development of materials science has been rapid, and the design and development of new types of functional materials have become an important engine to drive science and technology. Among these, gel materials have become ideal candidates for wearable electronic equipment, especially in flexible sensors. However, most gel materials tend to swell or degrade in wet environments, hindering their practical use. To address this problem, a novel strategy incorporating hydrophobic deep eutectic solvents (HESs) into gel networks is proposed, constructing a humidity-resistant eutectogel. Unlike previous studies that center upon hydrophobic modifications, this approach utilizes the unique properties of HESs to significantly enhance gel stability under humid conditions. This results in a gel material that not only resists swelling but also maintains its mechanical integrity and functionality over long periods (365 d in humid environments). Meanwhile, superior mechanical, adhesive, self-healing, temperature-tolerant, and antibacterial properties are achieved due to the strong noncovalent interactions between polymer chains and HESs. High sensitivity to strain, pressure, and temperature is realized, making the eutectogel suitable for multi-sensing applications.

1. Introduction

Recently, flexible sensors have attracted significant attention due to their great potential in artificial intelligence, soft robotics, health monitoring, and clinical care.[1–3] In particular, gel-based flexible sensors—such as hydrogels, organogels, ionogels, and eutectogels—show considerable promise because of their excellent conductivity, ductility, and other outstanding properties.[4–7] However, most gel-based flexible sensors are typically designed for use in open-air environments and are unsuitable for wet conditions.[8] This limitation mainly arises from the leakage of conductive molecules and the swelling behavior of the gels in humid environments.[9–11] Currently, commercially available gel-based sensors generally have a short lifespan under such conditions due to their poor humidity resistance. Therefore, it is crucial to develop gel-based sensors that remain stable in wet environments.

Deep eutectic solvents (DESs) are a subclass of eutectic mixtures characterized by thermodynamic non-ideality, in which components (typically Lewis or Brønsted acid–base pairs) exhibit enthalpy-driven negative deviations from ideality, resulting in a significant depression of the melting point.[12] DESs possess low volatility, high atom economy, good ionic conductivity, biocompatibility, and compatibility with gel networks, offering both flexibility and stretchability.[13,14] Eutectogels, typically composed of polymer networks and DESs, have been developed for a range of applications, including adhesives,[15–17] self-healing materials,[18,19] 3D printing materials,[20–22] batteries,[23,24] supercapacitors,[25–27] and flexible sensors.[28–30] However, many eutectogels fail to provide

[a] *Institute of Bast Fiber Crops, Chinese Academy of Agricultural Sciences, Changsha 410205, Hunan, P. R. China. E-mail: tanzhijian@caas.cn*

[b] *School of Materials Science and Engineering, Central South University, Changsha 410083, Hunan, P. R. China. E-mail: lihf@csu.edu.cn*

[c] *Shenzhen Branch, Guangdong Laboratory of Lingnan Modern Agriculture, Key Laboratory of Synthetic Biology, Ministry of Agriculture and Rural Affairs, Agricultural Genomics Institute at Shenzhen, Chinese Academy of Agricultural Sciences, Shenzhen, China. E-mail: caichangyong@caas.cn*

long-term detection of human physiological electrical signals in ambient or wet environments, primarily because most DESs are hygroscopic and sensitive to moisture.[31]

Hydrophobic DESs (HESs)—water-immiscible solvents composed of hydrophobic compounds—have recently gained attention in materials science.[32,33] Hydrophobic eutectogels, formed from HESs and polymer networks, show promise in addressing moisture sensitivity. The hydrophobic characteristics of HESs enhance the hydrophobicity of eutectogels, while their favorable properties contribute to improved gel performance. In summary, the development of eutectogels incorporating HESs opens new avenues for creating durable and humidity-resistant flexible electronic materials. Some eutectogels have been developed with HESs incorporated, exhibiting outstanding humidity-resistant performance.[8,16,34–37] However, they mainly focus on specific applications, including strain or pressure sensing, adhesion, or electrocardiogram (ECG) detection. Studies on their multifunctionality are also not comprehensive. For example, their self-healing and antibacterial properties are commonly lacking.

In this study, we propose a strategy to construct a novel humidity-resistant eutectogel with optimized multifunctionality and integrated multimodal sensing capabilities. Through strong non-covalent interactions, this eutectogel is readily synthesized *via* one-step photopolymerization of hydrophilic monomers in HESs. The inherent hydrophobicity of the HES inhibits ion transfer from the gel network, thereby ensuring both humidity resistance and ionic conductivity. We evaluated the optical and mechanical properties of the gel, as well as its adhesion, self-healing, antibacterial, and ionic conductive performance. Additionally, we explored its application in strain, pressure, and temperature sensing. This eutectogel offers a practical and effective solution for long-term humidity-resistant gel materials and lays a foundation for multifunctional sensing technologies.

2. Results and discussion

2.1. Design and fabrication of humidity-resistant eutectogels

First, tetrabutylammonium bromide (**TB**) and *n*-octanol (**O**) were mixed to create the HES **TBO**. Then, the acrylic acid (**A**) monomer underwent rapid one-step radical polymerization in the presence of the photoinitiator 2-hydroxy-2-methylpropiophenone within the HES under UV irradiation (365 nm) (Fig. 1a and Table S1, SI). The polymerization process was rapid and was completed in less than 30 s (Video S1, SI). A dual-barrier mechanism was developed to achieve humidity resistance: (a) **TBO** is intrinsically hydrophobic, acting as the first barrier; and (b) the **PA** network, with dense long-chain alkyl pendants (from **O**), limits water permeation, functioning as the second barrier. Moreover, the abundant carboxyl groups of **PA** enable multiple interactions with **TB**, facilitating ion transport responsive to strain, pressure, and temperature. The resulting **PA** network ensured mechanical integrity and adhesion. **TB** provides mobile quaternary ammonium cations and Br$^-$ anions, which contribute to both ionic conductivity and antibacterial properties. **O** acts as a hydrophobic
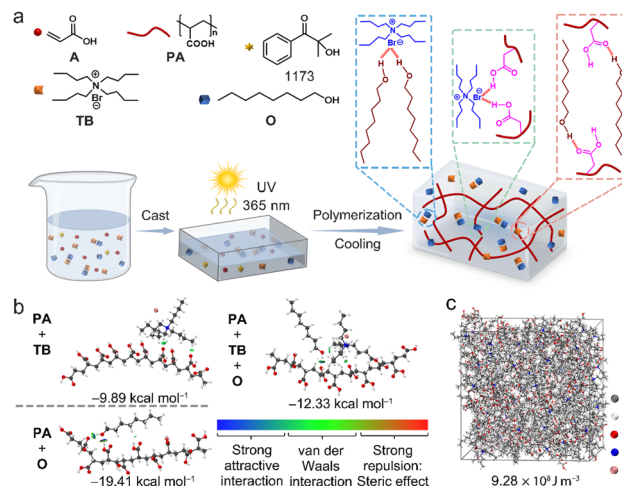

Fig. 1 Fabrication process and molecular calculation diagram of **PATBO**. (a) Schematic of the **PATBO** preparation process. (b) IGM isosurfaces and interaction energies among **PA**, **TB**, and **O**. (c) CED of **PATBO** with a **TBO** content of 60 wt%, calculated using 24 **PA** molecules, 72 **TB** molecules, and 144 **O** molecules.

moiety and a plasticizer, improving the hydrophobicity of the eutectogel, enhancing chain mobility for better stretchability, and contributing to a synergistic antimicrobial effect.

Theoretical calculations using the independent gradient model (IGM) revealed the interaction modes and energy decomposition results for **A**, **PA**, **TB**, and **O** (Fig. 1b, Fig. S1 and Table S2, SI). The **PATBO** eutectogel system relies primarily on hydrogen bonding, electrostatic interactions, and van der Waals forces, resulting in a low interaction energy of −12.33 kcal mol^{-1}.[38] If the synthesis process includes the crosslinker poly(ethylene glycol) diacrylate (**P**), an irreversible chemical crosslinking network is formed in the **PATBO** gel (Fig. S2, SI), which does not interfere with the reversible non-covalent interactions between **PA** and **TBO**. Additionally, theoretical calculations of the cohesive energy density (CED) were performed to determine the energy density per unit volume of **PATBO** (Fig. 1c and Fig. S3, SI).[39–41] The **PATBO** system with 60 wt% TBAB-OA demonstrated a high CED of 9.28×10^8 J m^{-3}. Various hydrophobic HES-based eutectogels were fabricated using a similar procedure (Tables S3 and S4, SI). The resulting **PATBO** eutectogel displayed a high transmittance of approximately 90% in the 400–800 nm range (Fig. S4, SI).

Fourier transform infrared (FTIR) and ^{1}H nuclear magnetic resonance (NMR) spectra confirmed the successful preparation of **TBO** HES and the **PATBO** eutectogel (Fig. S5 and S6, SI). In the FTIR spectra, the peak at 1630 cm^{-1}, corresponding to the C=C stretching vibration, disappeared for both the **PA** hydrogel and the **PATBO** eutectogel, indicating effective polymerization of the **A** monomers. The peak at 1694 cm^{-1}, attributed to the C=O stretching vibration of **PA**, exhibited a blue shift for both **PATBO** and **ATBO** compared to pure **PA**, suggesting molecular interactions between **A** and **TBO** (Fig. S5, SI).[42] In the ^{1}H NMR spectra, the downfield shifts in **TBO** protons (H$_a$: 0.741→0.772 ppm; H$_f$: 3.373→3.405 ppm) and upfield shifts in **PATBO** protons indicated altered electronic environments, consistent with molecular

interactions in the eutectic system (Fig. S6, SI). These spectroscopic changes confirmed the formation of a well-mixed eutectic system involving multiple interaction types.[43] The observed characterization results were consistent with simulation predictions.

### 2.2. Mechanical and ionic conductive properties of humidity-resistant eutectogels

Good mechanical properties are essential for eutectogels used in strain and pressure sensors. The mechanical performance of eutectogels composed of six different HESs and **PA** was evaluated. Among them, the **PATBO** eutectogel exhibited the highest tensile strength (2.43 MPa), toughness (10.84 MJ m^{-3}), and Young's modulus (339.33 kPa), along with excellent stretchability reaching 828.1% (Fig. S7 and Table S3, SI). Furthermore, the mechanical properties of **PATBO** with varying crosslinker **P** contents were also assessed. As the amount of **P** increased, the toughness and elongation at break decreased, while tensile strength increased (Fig. 2a and b). This behavior was mainly attributed to the more compact **PA** polymer network formed by additional **P**, which restricts polymer chain movement and limits energy dissipation *via* chain untwisting.[44] Additionally, the mechanical performance of **PATBO** with different HES contents was investigated. As the **TBO** content increased, elongation at break increased, whereas the tensile strength and toughness decreased (Fig. 2c and d). This can be explained by the looser network structure of **PATBO** at higher **TBO** contents, which allows greater polymer chain sliding and thus higher elongation. However, the lower density of non-covalent crosslinking reduces the strength and toughness of the

gel. For subsequent studies, **PATBO** containing 60 wt% HES and no crosslinker was selected for this study. Cyclic loading–unloading tests were conducted on the **PATBO** gel to assess its stretchability and self-recovery capacity (Fig. S8a and b, SI). The stress–strain curves exhibited repeatability owing to the self-restoration of the non-covalent bonds.[38] The dissipated energy (U_{hys}) increased with increasing strain, illustrating that the energy needed to fracture the eutectogel increased with increasing strain. This recovery behavior of the gel provided evidence for the presence of the dynamic attributes of hydrogen bonds.[29] The excellent energy dissipation and cyclic stability of **PATBO** were revealed by successive stretch-release tests at a strain of 300% (Fig. S8c and d, SI). A steep decrease in U_{hys} was observed after the first cycle, followed by a stepwise stabilization from the 2nd to the 10th cycle. This efficient energy dissipation may be attributed to the dynamic hydrogen bonding, ionic interactions, and hydrophobic association of the reversible **PATBO** eutectogel network structure.[29,45] The tensile stress remained relatively stable for 100 tensile loading–unloading cycles, indicating good tensile cyclic stability (Fig. 2e).

Similarly, **PATBO** exhibits the highest compressive strength among the six types of eutectogels, reaching 2.81 MPa at 70% strain (Fig. S9a, SI). As the **P** content increased, the compressive strength of **PATBO** increased (Fig. 2f). The compressive strength of **PATBO** improved because of the formation of a dense, chemically cross-linked polymer network. Furthermore, the compressive strength of **PATBO** increased as the **TBO** content decreased (Fig. 2g), because the **PATBO** eutectogel network structure became tighter, limiting the movement of the polymer chains. The cyclic compressive stability of a gel is critical to its electrochemical stability. The compressive stress–strain curves of **PATBO** show repeatability in consecutive cyclic compressive loading–unloading tests at 50% strain (Fig. S9b, SI). The dynamic hydrogen bond crosslinking in **PATBO** enables it to endure repeated compression. The compressive stress remained relatively stable over 100 loading–unloading cycles, demonstrating good compressive cyclic stability (Fig. 2h). In conclusion, **PATBO** eutectogels exhibited excellent tensile and compressive mechanical properties. Rheological tests showed that **PATBO** and all the other examined eutectogels exhibited typical elastic behavior. The storage modulus (G') was greater than the loss modulus (G'') (Fig. 2i and Fig. S10, SI).[46] Furthermore, all eutectogels exhibit ionic conductivity, and the ionic conductivity of the **PATBO** eutectogel is 0.85 S m^{-1} (Fig. S11, SI).

2.3. Adhesion, self-healing, temperature-tolerant, and antibacterial properties of humidity-resistant eutectogels

Good adhesion is essential for flexible wearable instruments. The high adhesion strength to the substrate endows the gel sensors with more stable and reliable signal recording. Macroscopic adhesion tests of **PATBO** revealed excellent adhesion to iron, copper, glass, poly(methyl methacrylate) (PMMA), polytetrafluoroethylene (PTFE), and human skin (Fig. S12 and Video S2, SI), with adhesion strengths measured using the lap shear test of 922.76 ± 82.85, 390.53 ± 27.44, 782.05 ± 44.64, 387.30 ± 88.76, and 218.26 ± 79.22 kPa (Fig. 3a). High adhesion
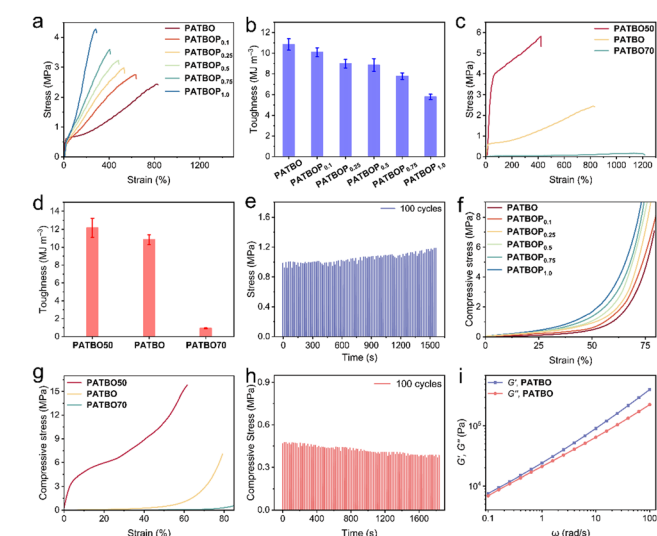
Fig. 2 Mechanical properties of the humidity-resistant eutectogels. (a) Tensile stress–strain curves and (b) corresponding toughness of **PATBO** eutectogels with various cross-linker contents. (c) Tensile stress–strain plots and (d) corresponding toughness of **PATBO** eutectogels with different TBAB-OA contents. (e) Tensile stress–time curves of PATBO during 100 loading–unloading cycles at 100% strain. (f) and (g) Compressive stress–strain curves of **PATBO** eutectogels with various cross-linker and TBAB-OA contents. (h) Compressive stress–time curves of **PATBO** during 100 loading–unloading cycles at 50% strain. (i) Rheological test of the **PATBO** eutectogel.
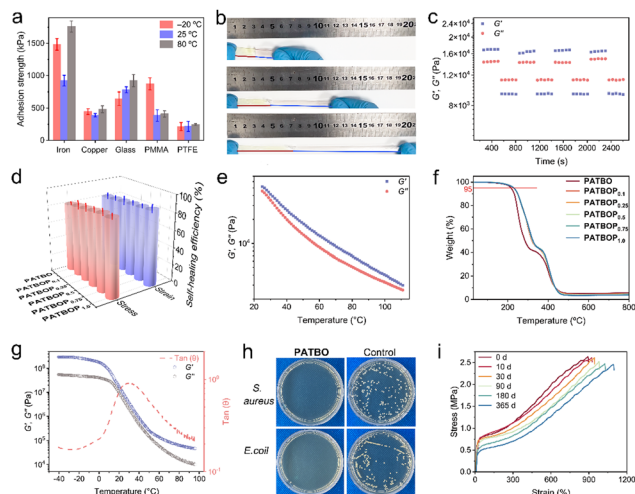
Fig. 3 Adhesion, self-healing, temperature-tolerant, and antibacterial characteristics of humidity-resistant eutectogels. (a) Adhesion strength of **PATBO** to various substrates at different temperatures (−20, 25, and 80 °C). (b) Visual images illustrating the self-healing behavior of **PATBO**. (c) Stepwise strain rheological tests performed on **PATBO** between low strain (0.1%) and high strain (100%). (d) Self-healing efficiencies of **PATBO** with varying **P** contents, showing recovery of tensile strength and elongation at break. (e) Rheological temperature ramp analysis of **PATBO**, demonstrating its thermal stability. (f) TGA spectra of **PATBO** with different **P** contents. (g) DMA spectra of **PATBO**. (h) Antibacterial properties of **PATBO**, revealed by photographs of colony-forming units. (i) Tensile stress–strain measurements of **PATBO** after exposure to 90% RH for different durations (0, 10, 30, 90, 180, and 365 d).

strengths were obtained under both cold (−20 °C) and hot (80 °C) conditions (Table S5, SI). The high adhesion strengths are due to the abundant hydroxyl groups of the **PATBO** gel system, which enable it to adhere to diverse substrates through multiple non-covalent interactions, such as hydrogen bonding, electrostatic attraction, ion–dipole interactions, and metal complexation.[45] Furthermore, the **PATBO** eutectogels exhibit excellent self-healing performance, as shown in the visual tests (Fig. 3b and Video S3, SI). Stepwise strain rheological tests, alternating between low strain (0.1%) and high strain (100%), illustrate the rapid and reversible gel–sol–gel transition of **PATBO**, highlighting its good self-healing properties (Fig. 3c).[38] Other eutectogels exhibit similar self-recovery ability (Fig. S13–S15, SI). The two separated gel segments were placed in contact at room temperature in a desiccator for 12 h with no applied external force, resulting in eutectogels with good self-healing efficiencies (HEs). The HE values of **PATBO** were 85.63% (strain) and 72.16% (stress) (Fig. 3d and Fig. S16, SI). The self-healing performance of **PATBO** can be primarily attributed to the synergistic effects of the eutectogel system. First is the dynamic hydrogen bonding between the carboxyl groups of **PA** and the hydroxyl groups of **O**/Br$^-$ of **TB**, as supported by FTIR analysis (Fig. S5, SI), ^{1}H NMR analysis (Fig. S6, SI), and IGM calculations (Fig. 1b). The second mechanism is the transient ionic interactions between the Br$^-$ anions of **TB** and the protonated **PA** chains. The DES environment, which is rich in hydrogen bond donors and acceptors, likely facilitates the reversibility of these interactions.

The temperature tolerance of gel-based flexible wearable sensors is important for their use under both hot and cold conditions. As illustrated by the rheological temperature ramp test, **PATBO** exhibits good anti-drying performance with G' always higher than G'', demonstrating its excellent elasticity between 25 and 110 °C (Fig. 3e and Fig. S17–S19, SI). Thermogravimetric analysis (TGA) confirmed this property, with the eutectogels showing a minimal weight loss at temperatures below 210 °C (Fig. 3f and Fig. S20, SI). Additionally, the **PATBO** eutectogel exhibited excellent anti-freezing properties. The dynamic mechanical analysis (DMA) of **PATBO** was performed from −40 to 100 °C, and no notable changes in G' and G'' were observed below 0 °C, illustrating its superior anti-freezing properties (Fig. 3g).[39] **PATBO** displays similar values of G' and G'' at different testing temperatures (−20, 0, 25, and 80 °C), indicating its good viscoelastic behavior, which is beneficial for gel-based sensors requiring energy dissipation and flexibility (Fig. S21, SI). Differential scanning calorimetry (DSC) tests were conducted from −100 to 100 °C, showing that the incorporation of **TBO** into the **PATBO** eutectogel can decrease the glass transition temperature from 48.59 °C (**PA** hydrogel) to −2.9 °C (Fig. S22, SI). This illustrates the excellent freezing resistance of **PATBO**.

Antibacterial performance is important for gel-based wearable sensors to ensure human health because they can resist external infections. Two methods were used to assess the antibacterial activity of **PATBO** against *Staphylococcus aureus* (*S. aureus*) and *Escherichia coli* (*E. coli*). The inhibition rates of both was 100%, demonstrating the superior ability of **PATBO** to inhibit bacterial growth (Fig. 3h and Fig. S23, SI). Quaternary ammonium **TB** can disrupt bacterial membranes through electrostatic interactions. Long-chain alcohol **O** can penetrate hydrophobic bacterial membranes and destabilize lipid bilayers. **PA** has a negative charge and can interact with the positive charges of the bacterial cell wall, interfering with the integrity of the cell membrane and leading to cell rupture or functional damage. These synergistic effects contribute to the antibacterial activity of **PATBO**. Furthermore, **PATBO** eutectogels exhibited remarkable humidity resistance. They demonstrated excellent tensile properties after storage at 90% RH for 365 d, which were comparable to the original properties (Fig. 3i). Additionally, only small changes in the eutectogel shape compared with the **PA** hydrogel were observed after long-term storage at 90% RH (Fig. S24, SI).

2.4. Application of PATBO as strain, pressure, and temperature sensors

Benefiting from several desirable properties, such as mechanical strength, ionic conductivity, adhesiveness, self-healing, temperature tolerance, antibacterial properties, and humidity resistance, **PATBO** eutectogels can be used as strain, pressure, and temperature sensors. First, their abilities to function as strain sensors were assessed. The gauge factor (GF), determined from the plot of the relative resistance changes ($\Delta R/R_0$) *versus* the applied strain, was used to evaluate the strain-sensing sensitivity of the **PATBO** sensors. The GF values of the **PATBO** strain sensor are 1.65, 1.78, 1.87, and 1.90 in the strain ranges of 0–100%, 100–200%, 200–300%, and 300–400% (Fig. 4a). The **PATBO** strain sensor

exhibited favorable performance in detecting both small (5%, 10%, 30%, 50%, and 70%) and large (100%, 200%, 300%, and 400%) strains (Fig. 4b and c). The $\Delta R/R_0$ values vary with strain levels, increasing with increasing strain. Furthermore, the **PATBO** strain sensor showed stable and consistent signal output at various tensile rates and at the same strain level (100%) (Fig. 4d). The **PATBO** eutectogels were subjected to 200 cycles of 100% strain tensile testing to evaluate the cyclic signal output of the strain sensors. The eutectogels demonstrated prominent stability, with the $\Delta R/R_0$ values remaining essentially the same with no significant differences (Fig. 4e). In addition, the **PATBO** strain sensors demonstrate superior sensing stability after storage in a wet environment (90% RH) for 30 and 180 d (Fig. 4f and Fig. S25, SI), indicating a high resistance to humidity. Practical application of the **PATBO** strain sensors demonstrates that they can detect both large- and small-scale movements of the human body and output signals in real time (Fig. 4g–l and Fig. S26, SI). The sensors were used to monitor the bending of the finger, elbow, knee, wrist, and ankle, displaying clear and consistent signal outputs corresponding to each movement (Fig. 4g–i and Fig. S26, SI). The signal amplitude increased proportionally with the bending angle, indicating high sensitivity to varying degrees of deformation. Additionally, the sensors can detect subtle facial movements, such as frowning, smiling, and swallowing, and displayed stable signal outputs in cyclic tests (Fig. 4j–l).
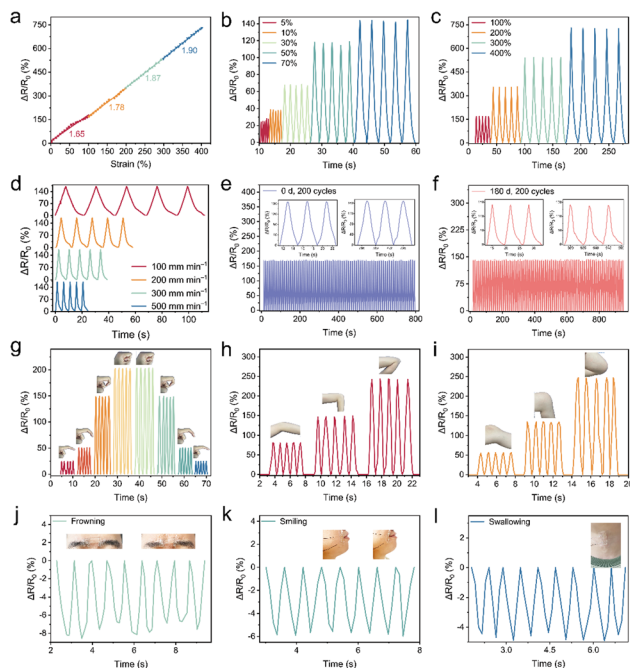

Fig. 4 Strain sensing properties and application of **PATBO** eutectogels as strain sensors. (a) Strain sensing sensitivity of **PATBO** as a strain sensor. (b) and (c) $\Delta R/R_0$ under (b) small and (c) large strains. (d) Stable $\Delta R/R_0$ outputs at varying tensile rates. (e) and (f) Strain sensing stability under 100% strain for 200 cycles after **PATBO** was stored in 90% RH for (e) 0 and (f) 180 d. (g)–(i) Practical application of **PATBO** strain sensors in detecting large-scale body movements: (g) bending finger, (h) bending elbow, and (i) bending keen. (j)–(l) Practical application of **PATBO** strain sensors in monitoring small-scale movements: (j) frowning, (k) smiling, and (l) swallowing.

The anti-swelling performance of the eutectogels was evaluated. The gel networks and shapes of **PATBO50**, **PATBO**, and **PATBO70** (without **P** as the crosslinker) were prone to underwater collapse. However, after reaching water equilibrium for 2 h, the swelling rates of **PATBOP$_{0.1}$**, **PATBOP$_{0.25}$**, **PATBOP$_{0.5}$**, **PATBOP$_{0.75}$**, and **PATBOP$_{1.0}$** are 29.10 $\pm$ 3.13%, 26.84 $\pm$ 3.43%, 24.39 $\pm$ 0.90%, 21.76 $\pm$ 0.73%, and 19.97 $\pm$ 2.43%, respectively (Fig. S27, SI). Improved anti-swelling abilities were correlated with the increased **P** content. A higher **P** content leads to a more compact polymer network, confining water absorption and preventing the collapse of the underwater structure. In contrast, the gels without **P** lacked sufficient chemical crosslinking points, which resulted in network disintegration upon swelling. So, **PATBOP$_{1.0}$** was chosen to investigate its application in underwater sensing and recording. As shown in Fig. S28, SI, it demonstrated excellent and stable human body sensing signal recording performance.

Next, the pressure sensing performance of the **PATBO** eutectogel was evaluated. The pressure sensitivity (SP), defined as the change in the current ($\Delta I/I_0$) with applied pressure, was used to assess the pressure-sensing ability of **PATBO** eutectogels.[29] The SP values vary with the pressure and are 1.32 kPa^{-1} (0–100 kPa), 1.47 kPa^{-1} (100–200 kPa), 1.52 kPa^{-1} (200–300 kPa), and 2.14 kPa^{-1} (300–500 kPa) (Fig. 5a). Pressure-sensing tests were conducted at both low (5, 10, 30, 50, and 70 kPa) and high (100, 200, 300, and 400 kPa) pressures, revealing the excellent sensing ability of **PATBO** and showing that $\Delta I/I_0$ increased with increasing pressure (Fig. 5b and c). The $\Delta I/I_0$ signal outputs at various pressing rates were stable and uniform at the same pressure (20 kPa) (Fig. 5d). The cyclic pressure sensing stability of the **PATBO** pressure sensors was tested over 250 compression cycles at 20 kPa. The $\Delta I/I_0$ signals remained relatively stable and steady (Fig. 5e). Even after storage at 90% RH for 30 to 180 d, the pressure-sensing properties remained stable, and the changes in $\Delta I/I_0$ were minimal compared to the original value (Fig. 5f and Fig. S29, SI). This illustrates the excellent pressure sensing stability and humidity resistance of **PATBO** eutectogels.

Finally, temperature sensing properties were investigated. The temperature sensitivity (ST) is determined from the plot of $\Delta R/R_0$ versus the temperature.[29] Two distinct ST values were obtained in the range of 30–100 °C: -2.82% °C^{-1} for 30–60 °C and -0.28% °C^{-1} for 60–100 °C (Fig. 5g). The $\Delta R/R_0$ values decreased stepwise with the temperature increments of 1 °C, with steady plateaus observed at each temperature level (Fig. 5h). This confirms the temperature sensing precision and stability of **PATBO**. A twelve-cycle alternating temperature measurement (30 and 60 °C) was performed, and the $\Delta R/R_0$ signal was cyclically stable, indicating the good cyclic temperature sensing stability of the **PATBO** sensor (Fig. 5i). The practical applications of the **PATBO** temperature sensor were evaluated. The sensor monitored the temperature of the palm and back of the hand in real time (Fig. 5j). Using an infrared thermal imager, the detected temperatures were 34.5 °C (back of the hand) and 35.0 °C (palm of the hand). The stable $\Delta R/R_0$ signals displayed by **PATBO** illustrated its exceptional temperature sensing precision. Compared to previously reported eutectogels, **PATBO** eutectogels offer more comprehensive combination of functional
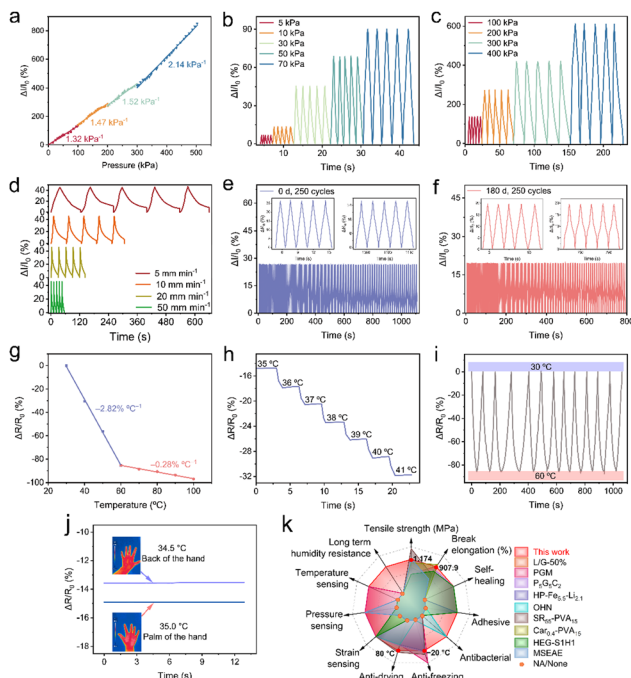
Fig. 5 Pressure and temperature sensing performances of **PATBO** eutectogels. (a) Pressure sensitivity of the **PATBO** pressure sensor, showing the relationship between $\Delta I/I_0$ and applied pressure. (b) and (c) $\Delta I/I_0$ under (b) low pressures (5, 10, 30, 50, and 70 kPa) and (c) high pressures (100, 200, 300, and 400 kPa). (d) Stable $\Delta I/I_0$ outputs at different pressing rates (5, 10, 20, and 50 mm min^{-1}) under 30 kPa. (e) and (f) Pressure sensing stability under 20 kPa for 250 cycles after storage at 90% RH for (e) 0 and (f) 180 d. (g) Temperature sensitivity of the **PATBO** sensor, illustrating the correlation between $\Delta R/R_0$ and applied temperature. (h) $\Delta R/R_0$ responses as temperature increases from 25 to 41 °C at 1 °C intervals. (i) Temperature sensing stability across 12 cycles between 30 and 60 °C. (j) Real-time body temperature monitoring on the palm and back of the hand. (k) Comparisons of **PATBO** with other reported eutectogels across 11 performance aspects, including tensile strength, adhesion, antibacterial activity, and humidity resistance.

properties—including mechanical, adhesive, self-healing, antibacterial, anti-freezing, and anti-drying capabilities—as well as versatile sensing performance for strain, pressure, and temperature (Fig. 5k and Table S6, SI).[28,29,34,35,37,47–50]

3. Conclusions

A transparent and humidity-resistant eutectogel was successfully fabricated by rapidly and cost-effectively copolymerizing A monomers in a HES matrix under UV irradiation. The resulting eutectogel exhibited high optical transparency (approximately 90% transmittance in the visible light range), strong adhesion (up to 922.76 kPa on iron), excellent self-healing performance (81.16 ± 4.13% recovery in strain and 80.34 ± 2.46% in stress), and outstanding resistance to freezing (−20 °C), drying (80 °C), and bacterial contamination (100% inhibition against two bacterial strains). Furthermore, the tensile mechanical properties (with 99.3% toughness retained) and the shape of the prepared eutectogel showed nearly no change after storage in a wet environment (90% RH) for 365 d. Based on these results, a

eutectogel-based strain, pressure, and temperature sensor was developed. This multifunctional sensor illustrated excellent sensing sensitivity and signal output stability. Moreover, the eutectogel sensor demonstrates superior cyclic strain and pressure sensing stability, even after being placed in a humid atmosphere for 180 d. These results not only highlight the durability and versatility of the **PATBO** eutectogel but also provide a promising foundation for the development of next-generation functional gel materials in wearable electronics and related applications.

Author contributions

Z. T. and H. L. supervised the project and designed the experiments. Q. L. performed all the experiments and characterization. Q. L. and C. C. analyzed the data and participated in the writing of the manuscript. All authors commented on the manuscript.

Conflicts of interest

There are no conflicts to declare.

Data availability

The data supporting this article have been included as part of the SI. The SI file contains additional data and materials that support the findings presented in the main text of the manuscript. Specifically, it includes detailed materials and experimental methods. Theoretical calculation details used in the study. Supplementary tables, figures, and videos that provide further clarification of key results. See DOI: **https://doi.org/10.1039/d5mh01293g**

Acknowledgements

Notes and references

1 H. Jang, J. Lee, C. J. Beak, S. Biswas, S. H. Lee and H. Kim, *Adv. Mater.*, 2025, **37**, 2416073.
2 S. Davies, Y. Hu, N. Jiang, J. Blyth, M. Kaminska, Y. Liu and A. K. Yetisen, *Adv. Funct. Mater.*, 2021, **31**, 2105645.
3 M. Kim, S. Hong, R. Khan, J. J. Park, J. B. In and S. H. Ko, *Small*, 2025, **21**, 2405301.
4 J. Yang, Y. Yan, L. Huang, M. Ma, M. Li, F. Peng, W. Huan and J. Bian, *ACS Nano*, 2025, **19**, 2171–2184.

5 H. Song, D. H. Jung, Y. Cho, H. H. Cho, V. G. Panferov, J. Liu, J. H. Heo and J. H. Lee, *Coord. Chem. Rev.*, 2025, **541**, 216835.

6 A. Roy, S. Zenker, S. Jain, R. Afshari, Y. Oz, Y. Zheng and N. Annabi, *Adv. Mater.*, 2024, **36**, 2404225.

7 E.-I. Lee, H.-J. Ko, J. Kim and J.-W. Park, *Nano Energy*, 2025, **139**, 110984.

8 D. Du, J. Zhou, T. Kaneko, W. Dong, M. Chen and D. Shi, *Chem. Eng. J.*, 2023, **474**, 145704.

9 X. Zhou, X. Zhao, Y. Wang, P. Wang, X. Jiang, Z. Song, J. Ding, G. Liu, X. Li, W. Sun and W. Xu, *Composites, Part B*, 2023, **255**, 110631.

10 C. Sun, J. Luo, T. Jia, C. Hou, Y. Li, Q. Zhang and H. Wang, *Chem. Eng. J.*, 2022, **431**, 134012.

11 X. Ma, X. Zhou, J. Ding, B. Huang, P. Wang, Y. Zhao, Q. Mu, S. Zhang, C. Ren and W. Xu, *J. Mater. Chem. A*, 2022, **10**, 11823–11853.

12 D. O. Abranches and J. A. P. Coutinho, *Annu. Rev. Chem. Biomol. Eng.*, 2023, **14**, 141–163.

13 P. A. Mercadal, A. González, A. Beloqui, L. C. Tomé, D. Mecerreyes, M. Calderón and M. L. Picchio, *JACS Au*, 2024, **4**, 3744–3758.

14 B. B. Hansen, S. Spittle, B. Chen, D. Poe, Y. Zhang, J. M. Klein, A. Horton, L. Adhikari, T. Zelovich, B. W. Doherty, B. Gurkan, E. J. Maginn, A. Ragauskas, M. Dadmun, T. A. Zawodzinski, G. A. Baker, M. E. Tuckerman, R. F. Savinell and J. R. Sangoro, *Chem. Rev.*, 2021, **121**, 1232–1285.

15 K. Zhang, R. a Li, G. Chen, X. Wang and M. He, *Chem. Mater.*, 2022, **34**, 3736–3743.

16 J. L. de Lacalle, M. L. Picchio, A. Dominguez-Alfaro, R. R.-M. Serrano, B. Marchiori, I. D. Agua, N. Lopez-Larrea, M. Criado-Gonzalez, G. G. Malliaras and D. Mecerreyes, *ACS Mater. Lett.*, 2023, **5**, 3340–3346.

17 M. B. Bianchi, C. Zhang, E. Catlin, G. Sandri, M. Calderón, E. Larrañeta, R. F. Donnelly, M. L. Picchio and A. J. Paredes, *Mater. Today Bio*, 2022, **17**, 100471.

18 R. A. Li, T. Fan, G. Chen, K. Zhang, B. Su, J. Tian and M. He, *Chem. Mater.*, 2020, **32**, 874–881.

19 M. Criado-Gonzalez, N. Alegret, A. M. Fracaroli, D. Mantione, G. Guzmán-González, R. Del Olmo, K. Tashiro, L. C. Tomé, M. L. Picchio and D. Mecerreyes, *Angew. Chem., Int. Ed.*, 2023, **62**, e202301489.

20 C. Zhang, H. Zheng, J. Sun, Y. Zhou, W. Xu, Y. Dai, J. Mo and Z. Wang, *Adv. Mater.*, 2021, **34**, 2105996.

21 R. Ruiz-Mateos Serrano, A. Aguzin, E. Mitoudi-Vagourdi, X. Tao, T. E. Naegele, A. T. Jin, N. Lopez-Larrea, M. L. Picchio, M. Vinicio Alban-Paccha, R. J. Minari, D. Mecerreyes, A. Dominguez-Alfaro and G. G. Malliaras, *Biomaterials*, 2024, **310**, 122624.

22 S. Nechausov, Y. Jiang and A. Miriyev, *Addit. Manuf.*, 2025, **104**, 104743.

23 Y. Zheng, D. Wu, T. Wang, Q. Liu and D. Jia, *Angew. Chem., Int. Ed.*, 2024, **64**, e202418223.

24 C. Gu, M. Wang, K. Zhang, J. Li, Y. L. Lu, Y. Cui, Y. Zhang and C. S. Liu, *Adv. Mater.*, 2022, **35**, 2208392.

25 Y. Bai, X.-F. Zhang, Y. Wu, H. Liu and J. Yao, *J. Mater. Chem. A*, 2024, **12**, 28307–28314.

26 Q. Zeng, X. Lai, H. Li, Z. Chen, X. Zeng and L. Zhang, *Adv. Funct. Mater.*, 2024, **34**, 2411029.

27 Y. Han, B. J. So, H. J. Kim, J. H. Kim, J. H. Lee, G. Shin, J. Y. Baek, H. Kim, M. W. Lee, S. K. Moon, K.-B. Seo, S. Y. Park, J. G. Jeon, H. Shin and T. J. Kang, *Energy Storage Mater.*, 2024, **64**, 103070.

28 Y. Sun, Y. Cheng, L. Shi, J. Sun, S. Chen and R. Wang, *Adv. Funct. Mater.*, 2024, **34**, 2101808.

29 B. Guo, M. Yao, S. Chen, Q. Yu, L. Liang, C. Yu, M. Liu, H. Hao, H. Zhang, F. Yao and J. Li, *Adv. Funct. Mater.*, 2024, **34**, 2315656.

30 T. H. Vo, P. K. Lam, R.-M. Chuang, F.-K. Shieh, Y.-J. Sheng and H.-K. Tsao, *Chem. Eng. J.*, 2024, **493**, 152877.

31 Y. Wan, S. Huang, Y. Sun, H. Zhu, Q. Zheng, Q. Zhang and S. Zhu, *Chem. Eng. J.*, 2022, **442**, 136289.

32 D. J. G. P. van Osch, C. H. J. T. Dietz, S. E. E. Warrag and M. C. Kroon, *ACS Sustainable Chem. Eng.*, 2020, **8**, 10591–10612.

33 M. Marchel, M. P. Rayaroth, C. Wang, L. Kong, J. A. Khan and G. Boczkaj, *Chem. Eng. J.*, 2023, **475**, 144971.

34 C. Chai, L. Ma, Y. Chu, W. Li, Y. Qian and J. Hao, *J. Colloid Interface Sci.*, 2023, **638**, 439–448.

35 X. Zhang, S. Liu, X. Wang, J. Peng, W. Yang, Y. Ma and K. Fan, *J. Colloid Interface Sci.*, 2024, **654**, 1348–1355.

36 K. Yang, Z. Ge, M. Zhang, C. Wang, K. Peng, H. Yang and Y. You, *Chem. Eng. J.*, 2022, **439**, 135646.

37 M. Li, Z. Liu, Y. Hu, R. A. Li and Y. Cao, *Chem. Eng. J.*, 2023, **472**, 145177.

38 Q. Lu, H. Li and Z. Tan, *J. Mater. Chem. A*, 2024, **12**, 20307–20316.

39 C. Cai, H. Gong, S. Wu, F. Li, S. Liu, Z. Tan and S. Dong, *Chem. Eng. J.*, 2023, **451**, 138674.

40 Q. Lu, H. Li and Z. Tan, *Carbohyd. Polym.*, 2025, **348**, 122939.

41 C. Cai, Y. Pan, Y. Zhang, F. Li, Z. Tan and S. Dong, *CCS Chem.*, 2025, **7**, 2520–2530.

42 R. Xue, N. Zhou, S. Yin, Z. Qian, Z. Dai and Y. Xiong, *Chem. Eng. J.*, 2023, **465**, 143072.

43 D. O. Abranches, L. P. Silva, M. A. R. Martins, S. P. Pinho and J. A. P. Coutinho, *ChemSusChem*, 2020, **13**, 4916–4921.

44 P. Wang, D. Pei, Z. Wang, M. Li, X. Ma, J. You and C. Li, *Chem. Eng. J.*, 2020, **398**, 125540.

45 P. Yao, Q. Bao, Y. Yao, M. Xiao, Z. Xu, J. Yang and W. Liu, *Adv. Mater.*, 2023, **35**, 2300114.

46 Y. Liang, K. Wang, J. Li, H. Wang, X. Q. Xie, Y. Cui, Y. Zhang, M. Wang and C. S. Liu, *Adv. Funct. Mater.*, 2021, **31**, 2104963.

47 Y. Wang, S. Fu, L. A. Lucia and H. Zhang, *Compos. Sci. Technol.*, 2022, **229**, 109696.

48 S. Chen and J. Feng, *ACS Appl. Mater. Interfaces*, 2023, **15**, 44752–44762.

49 T. H. Vo, P. K. Lam, T.-F. Hsiao, C.-J. M. Chin, Y.-J. Sheng and H.-K. Tsao, *J. Colloid Interface Sci.*, 2024, **659**, 495–502.

50 J. Liu, L. Zhou, P. Zhang, Y. Zhao, H. Wei and Y. Yu, *CCS Chem.*, 2024, **6**, 390–402.